

Fast, Scalable, Energy-Efficient Non-element-wise Matrix Multiplication on FPGA

Xuqi Zhu, Huaizhi Zhang, JunKyu Lee, Jiacheng Zhu, Chandrajit Pal, Sangeet Saha,
Klaus D. McDonald-Maier and Xiaojun Zhai

Abstract—Modern Neural Network (NN) architectures heavily rely on vast numbers of multiply-accumulate arithmetic operations, constituting the predominant computational cost. Therefore, this paper proposes a high-throughput, scalable and energy-efficient non-element-wise matrix multiplication unit on FPGAs as a basic component of the NNs. We firstly streamline inter-layer and intra-layer redundancies of MADDNESS algorithm, a LUT-based approximate matrix multiplication, to design a fast, efficient scalable approximate matrix multiplication module termed “Approximate Multiplication Unit (AMU)”. The AMU optimizes LUT-based matrix multiplications further through dedicated memory management and access design, decoupling computational overhead from input resolution and boosting FPGA-based NN accelerator efficiency significantly. The experimental results show that using our AMU achieves up to $9\times$ higher throughput and $112\times$ higher energy efficiency over the state-of-the-art solutions for the FPGA-based Quantised Neural Network (QNN) accelerators.

Index Terms—Approximate Matrix multiplier, QNN, Neural network accelerator, FPGA

I. INTRODUCTION

Recent years have been notable progress in the field of hardware-based inference accelerators implementing Neural Networks (NNs) for AI [1]. As such AI application scenarios continue to broaden, addressing diverse performance-oriented requirements for varying tasks emerges as a new challenge [2], [3], [4]. To handle the diversity of AI applications and the sophistication of task scenarios, researchers are exploring the design of performance-scalable multipliers in NN accelerators executing AI applications at varying scales and performance requirements for simplification. For example, an IoT application for facial recognition utilising Floor of Log achieves high efficiency in terms of energy utilisation and storage while maintaining an acceptable decrement in accuracy. On the other hand, some health and activity monitoring applications require high accuracy at the cost of high energy consumption in inferring user activities by utilizing sophisticated sensors, features, and complex classification algorithms that lead to higher energy consumption. Another example is the use of any-precision NN that prioritises accuracy at the cost of an increased execution time or energy consumption [5], [6], [7]. Together, these sources highlight the complex trade-offs that NNs undergo to balance model complexity, accuracy, execution time, and energy consumption. This emphasises the

necessity of thorough analysis and optimisation to strike the right balance for particular applications and environmental factors.

Numerous studies have explored resource-efficient, high-throughput solutions on NN accelerators for diverse range of AI applications and complex task scenarios [8]. Since matrix multiplication is a major computational overhead in NN inference tasks, an optimized matrix multiplication unit can improve the overall accelerator performance. Several studies used quantised matrices to simplify multiplication computation and memory requirements. Authors in [9] proposed FP-BNN, a binarized neural network, by replacing the exact multiplication with XNOR and Pop-count operation. Similarly, authors in [10], [11] substituted the matrix multiplication operation with a computational unit, a.k.a. Matrix Vector Activation Unit (MVAU), using XNOR and Pop-count operations. By sacrificing a bit of accuracy performance, the MVAU can achieve much faster processing speed and lower resource utilization. Since bit operations are well-suited to FPGA hardware logic, MVAU has been recognized as an effective solution for accelerating BNN inference [12]. Wang et al. [13] introduced LUT-Net, aiming to enhance the logic density of XNOR gate-based matrix multiplication. Zhang et al. [14] developed FracBNN, a novel BNN architecture designed to mitigate accuracy degradation caused by low-precision quantization in XNOR gate-based matrix multiplication. Blalock et al. [15] proposed the MADDNESS, a LUT-based matrix multiplication algorithm, to speed up matrix multiplications while using fewer compute resources. MADDNESS leverages a form of Product Quantization (PQ) [16], [17] that organizes datasets into a fixed number of clusters and learns substitutes for the sample vectors within each cluster. This approach achieves notable acceleration with a minor loss of accuracy in NN inference tasks. This method has been further leveraged in NN inference works [18], [19].

Efficient accelerators depend not only on individual matrix multiplication units but also on the design of the overall computing architectures. For example, FINN [10], [11], an FPGA-based end-to-end deployment tool for QNN accelerator, leverages streamlined technique [20] to achieve a certain level of customization on parallelism and resource utilization by introducing matrix folding strategies. Similarly, HLS4ML [21], FlexCNN [22], Angel-Eye [23], DNNBuilder [24] and HybridDNN [25] provided alternative frameworks for an FPGA-oriented end-to-end deployment tool for NN accelerator. Beyond targeting FPGA platforms, HEP-BNN [26] is a BNN accelerator framework, that can automatically generate

All authors are with the School of Computer Science and Electronic Engineering, University of Essex, Colchester CO4 3SQ, United Kingdom. E-mails: {xz18173, hz24245, j.lee, jz23222, chandrajit.pal, sangeet.saha, kdm, xzhai}@essex.ac.uk

an efficient layer-to-device mapping for GPUs and CPUs. The studies in [18], [19], [27] illustrated an ASIC accelerator for NN inference applications on x86 server CPU.

However, the solutions proposed in the aforementioned studies did not address the challenges posed by varying problem sizes in matrix multiplication operations, leading to degraded accelerator throughput and energy efficiency, especially with larger problem sizes. *First, element-wise arithmetic operations serve as the primary performance bottleneck for matrix multiplications, leading to $O(n_m^3)$ computational complexity, where n_m is the matrix size.* Although some methods, such as folding strategy [20], offer a scalable performance through tuning parallelism and resource utilization, XNOR gate-based matrix multiplication still requires a considerable amount of element-by-element arithmetic operations. This will then result in inevitable computation and data access cost, affect the efficiency and prevent matrix multiplication units such as MVAU [10], [11], from achieving better Pareto optimal on throughput and resource utilization. *Secondly, the previous approaches did not address software-hardware co-design optimization sufficiently for the specific algorithm's atypical logic behaviours.* The authors in [18], [19] used an approximate matrix multiplication algorithm having a completely different logic behaviour from the exact matrix multiplication operations, which introduced a significantly larger parameter size and atypical memory access behaviours to the NN models and NN accelerator. These pose a challenge in designing an efficient hardware accelerator.

The limitations of prior works motivated us to design a multiplier that can decouple the multiplication computation overhead from the size of the input feature map, enabling flexible tuning of the resources, accuracy and energy efficiency of the multiplier, ultimately improving NN accelerator performance. In this paper, we thus design an FPGA-based vector-matrix multiplication unit, termed the Approximate Multiplication Unit (AMU), which forsakes element-by-element arithmetic operations to decouple the multiplication computation overhead from the resolution of the input feature map (i.e., the problem size). This approach allows the AMU-based NN accelerator to achieve significant gains in throughput and energy efficiency, compared to the typical element-wise matrix multipliers. The AMU is an alternative arithmetic operation of MVAU, which can be used to build a resource-accuracy-efficiency scalable and latency invariant accelerator substituting the element-by-element arithmetic operation with the assistance of LUT-based storage.

The contributions of this paper are summarised as follows:

- We firstly streamline inter-layer and intra-layer redundancies of the MADDNESS-based matrix multiplication to enable a fast, efficient scalable approximate matrix multiplication on an FPGA-based QNN accelerator.
- We eliminate element-by-element arithmetic operations of matrix multiplication by introducing three optimization strategies (i.e., I/O data pruning, feature map reorganization, and parameter compression) on MADDNESS-based matrix multiplication to decouple the multiplication computation overhead from the problem size, which significantly improves the performance of the MADDNESS-based matrix multiplication.

- We explore the hardware design space on FPGA to optimize atypical memory allocation and access arising from the unstructured pruning on MADDNESS-based matrix multiplication.
- The proposed AMU-based NN inference accelerator achieves up to $9.9\times$ throughput and $112\times$ energy efficiency (GOPS/W) over the state-of-the-art solutions for FPGA-based Quantised Neural Network (QNN) accelerator with the same level of NN model complexity.

The overview of the proposed AMU is discussed in Section III, while Section IV presents the performance comparing between AMU and prior works, Section V discusses the conclusion and future challenge of our work.

II. APPROXIMATE MULTIPLICATION: MADDNESS [15]

This section firstly introduces the approximate multiplication method MADDNESS [15], preparatory to discussing our algorithm. MADDNESS is a LUT-based approximate multiplication algorithm, requiring offline training as shown in Fig. 1. (b). In the offline training, MADDNESS generates codebooks which will be used in the online multiplication stage.

A. Approximate multiplication setting for neural networks

The problem domain we are addressing in approximate multiplications on the two matrices, \mathbf{A} and \mathbf{W} , is outlined as follows:

$$\tilde{f}(\mathbf{A}, \mathbf{W}) = \mathbf{A} \times \mathbf{W} + \mathbf{E}, \quad (1)$$

where $\mathbf{A} \in \mathcal{R}^{n \times m}$, $\mathbf{W} \in \mathcal{R}^{m \times d}$, and the error matrix $\mathbf{E} \in \mathcal{R}^{n \times d}$. The $\|\mathbf{E}\|_2$ should be small enough according to the accuracy requirements.

For neural networks, \mathbf{A} can be represented as follows:

$$\mathbf{A}^T = [\mathbf{a}_1, \mathbf{a}_2, \dots, \mathbf{a}_n], \quad (2)$$

where $\mathbf{a}_i \in \mathcal{R}^n$. Each \mathbf{a}_i can be considered as the neuron values of the input layer in a fully connected layer. We utilize a pre-trained neural network (i.e., the weights \mathbf{W} are known).

Fig. 1. (a) describes a fully connected layer in a neural network, where $w_{j,k}$ represents a weight linking the j^{th} neuron in the previous layer to the k^{th} neuron in the current layer. The signal s_j entering each ReLU unit in Fig. 1.(a) follows Eq. (3):

$$s_j = \sum_{i=1}^{n_{in}} (w_{i,j} \times a_i) = (\mathbf{W}^T \mathbf{a}_{in})_j, \quad (3)$$

where \mathbf{a}_{in} is the neuron values in the input layer, $(\cdot)_j$ is the j -th component of a vector, n_{in} is the number of neurons at the input layer (e.g., the length of the vector \mathbf{a}), $\mathbf{W} = [\mathbf{w}_1, \mathbf{w}_2, \dots, \mathbf{w}_{n_{out}}]$, where $\mathbf{w}_i = [w_{i,1}, w_{i,2}, \dots, w_{i,n_{in}}]$, and n_{out} is the number of neurons at the output layer. The signals s_j are input signals for activation functions (i.e., ReLU). We name a series of input neurons $[a_1, a_2, \dots, a_m]^T$ as an input feature vector \mathbf{a}_{in} in this paper. Therefore, our approximate multipliers are focused on the multiplications between neurons and weights in a fully connected layer based on Eq. (3).

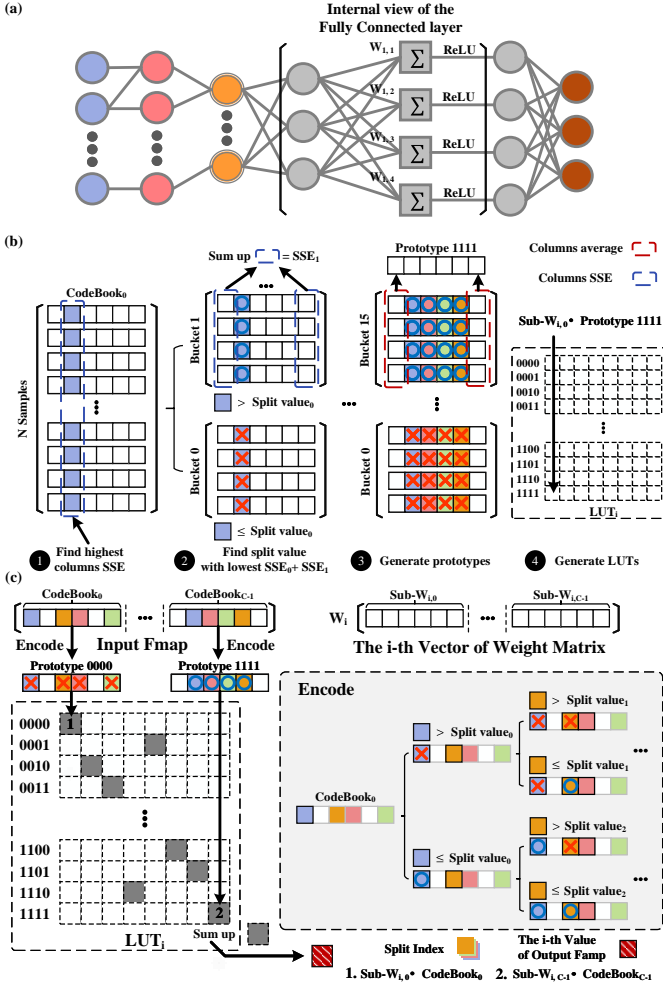


Fig. 1. (a) Fully connected layer, (b) MADDNESS offline training and (c) MADDNESS online multiplications

B. Offline training

We refer to “offline training” in this paper as the process used to compute partial dot product values in LUTs, distinct from the typical training method involving backpropagation used for training neural networks. In the first stage of the offline training, MADDNESS generates codebooks. Each codebook consists of a set of prototypes learned from training data. For example, using the i -th training sample, $\mathbf{a}_i \in \mathcal{R}^n$ can be divided into C $\mathcal{R}^{n/C}$ dimensional data, where C is an integer that allows $n/C = d_{sub}$ to be an integer. In this case, there exist C codebooks according to C sub-dimensions of training data. We use the notation $\mathbf{a}_i^{(c)}$ for the c -th sub-dimensional vector in the i -th training sample:

$$\mathbf{a}_i^{(c)} = [a_{1(i)}^{(c)}, \dots, a_{d_{sub}(i)}^{(c)}]. \quad (4)$$

To simplify without loss of generality, let us denote \mathbf{a} for $\mathbf{a}_i^{(c)}$ in this sub-section. MADDNESS uses a heuristic clustering strategy based on a decision tree to find a series of prototypes in each codebook. The clustering utilizes the hyperplane bisection method. For instance, the 1-st hyperplane generates 2^1 sub-spaces. Each sub-space is divided by its own hyperplane. Therefore, utilizing the h -th 2^{h-1} hyper-planes

create 2^h sub-spaces in the c -th codebook to classify the c -th sub-dimensional vectors across all training samples into 2^h sub-spaces. Considering all past buckets, the number of buckets in total becomes $n_b = \sum_{i=1}^I 2^i$, where I is the number of split indexes. Numbering buckets follows from left to right. For example, the first hyperplane generates the left-side sub-space (i.e., $a_{j_1} \leq v_1$, 1st bucket) and the right-side sub-space (i.e., $a_{j_1} > v_1$, 2nd bucket). We denote $j_{j'}$ for the j' -th split index.

The prototype for each bucket in a codebook can be considered as a representative vector for all sub-dimensional vectors assigned to that bucket. The prototype is found using the least squares algorithm. We use the notation $\mathbf{p}_{k,j_{j'}}^{(c)}$ to indicate the prototype for the k -th bucket in the c -th codebook generated by the split index $j_{j'}$.

For example, in Fig. 1. (b), the second element in sub-dimensional vectors, a_2 , is chosen for a hyperplane bisection. The hyperplane, $a_2 = v_0$ (Split value₀), splits sub-dimensional vectors into two sub-spaces across all training samples (i.e., the space where $a_2 > v_0$ and the other space where $a_2 \leq v_0$). Each split index divides the space into two sub-spaces. For example, the first split index splits the space into two sub-spaces and the next index divides each subspace into two sub-spaces, generating four sub-spaces in total. Similarly, n_h dimensions generate 2^{n_h} sub-spaces. Each subspace is referred to as a bucket in this paper. The $2^{j'-1}$ split values for the j' -th split index are determined heuristically so that they minimize the sum of squared errors between the $2^{j'}$ chosen prototypes and sub-dimensional vectors of training samples residing in the $2^{j'}$ buckets split by $2^{j'-1}$ split values in $\mathbf{v}_{j'} = [v_1, v_2, \dots, v_{2^{j'-1}}]^T$.

This process is performed in order from $k = 1$ to $k = n_b$. For example, $\mathbf{v}_1 = [v_1]$ is found for $k = \{1, 2\}$ (i.e., Buckets 0 ($k=1$) and 1 ($k=2$) in Fig. 1.(b)). After that, the first element in \mathbf{v}_2 is found for $k = \{3, 4\}$ and the second element is found when $k = \{5, 6\}$, and so on. In Fig. 1.(b), the first element in \mathbf{v}_4 is found for $k = \{15, 16\}$ (Buckets 0 and 1 in the last level of the tree) and the 8-th element is found for $k = \{29, 30\}$ (Buckets 14 and 15 in the last level of the tree). The binary decision tree finds suitable values that can split two children’s buckets from a father’s bucket with the lowest accumulated Sum of Squared Error (SSE) in MADDNESS. The initial prototypes are found by averaging the sub-dimensional vectors residing in the associated buckets. The least squares algorithm is used to find the final prototypes $\mathbf{p}_{k,j_{j'}}^{(c)}$ by refining the initial prototypes to minimize residuals further.

Once all prototypes are found, MADDNESS generates the LUTs containing dot-product values. Each row in a LUT represents a dot-product value between a prototype and a sub-dimensional *known* vector (e.g., a sub-dimensional weight vector). For example, in Fig. 1. (b), all possible partial dot product results between every prototype in each codebook and the sub-vectors of each dimension on the weight matrix (i.e., $\text{Sub-}W_{i,j}$) are computed and recorded in LUTs offline. Therefore, a LUT consists of a table having the size of $2^I \times C$. If the number of split indexes $I = 4$, each row element

contains the dot product value between the prototype in one of the last level buckets and one of the C sub-dimensional weight vectors.

C. Online multiplications (Inference)

Online multiplications assume that the patterns in the test dataset are similar to the training dataset. Under this assumption, we can utilize the LUTs generated from the offline training stage for the online multiplications.

In the online multiplication stage, a test sample is first divided into C sub-dimensional vectors. A partial dot product between a sub-dimensional test vector and a sub-dimensional weight vector is immediately found by referring to an LUT. For example, each grey cell in Fig. 1. (c) represents the partial dot product value between a prototype and a sub-dimensional weight vector. Since the first sub-dimensional test vector (i.e., the first block in Input Fmap) is mapped with the first prototype in $CodeBook_0$ and uses ‘1’ stored in the LUT for a partial product. Only the values at the four split indexes in a sub-dimensional test vector are referred to for the mapping procedures in Fig. 1. (c). Likewise, the second sub-dimensional vector is then mapped with the third prototype in the second codebook, and so on. Since a LUT contains a partial dot product value associated with each sub-dimension, the final dot product value can be thus found by adding the values in all grey boxes.

The right side in Fig. 1. (c) shows how to find the best prototype for each sub-dimensional vector in a test sample using the values in the split indexes. The binary decision tree generated in the offline training stage is leveraged to seek the best prototype. For example, the decision tree has the split index information and their values. At the outset, the first split index and its corresponding value within a sub-dimensional test sample determine the assignment of that vector to one of two buckets ($k = 1$ or 2). If the value at the split index of the test sample is less than the split value, it belongs to the left child bucket ($k = 1$). Subsequently, the second split index is assessed. If the value at the second index of the test sample exceeds the split value, it is assigned to the right bucket in the second level of the tree ($k = 4$). This binary tree search process persists until reaching the leaf nodes. Hence, I binary decisions are necessary for mapping. This can be realized by utilizing I bits as a LUT address. In Fig. 1. (c), for instance, the binary decisions derived from the split indexes of the first sub-dimensional vector are “XXXX” (equivalent to “0000”), while those from the last sub-dimensional vector are “OOOO” (equivalent to “1111”), serving as the LUT address for a partial dot product value. This prototype search is called encoding [15]. Therefore, MADDNESS can approximate matrix multiplications in the inference stage using LUTs, each representing a series of partial dot products.

III. APPROXIMATE MULTIPLICATION UNIT

To make the accelerator performance independent from the resolution of the input feature map (i.e., problem size), we designed a matrix multiplier, AMU, which improves MADDNESS [15] using the following three optimisation strategies: Input/Output data pruning, reorganising feature maps, and compressing LUT bespoke to hardware.

A. Challenges posed by MADDNESS

Although the original MADDNESS algorithm streamlines processing by eliminating the need for online matrix multiplication operation, it still requires element-by-element operations to produce all output elements, thereby introducing unnecessary inter-layer information transfer and redundant intra-layer parameters. For example, a matrix-vector multiplication in Eq. (3) requires n_{out} dot products (i.e., MADDNESS is required to compute all s_j in Eq. (3).), failing to alleviate the time and space complexities associated with the input feature map resolution (i.e., problem size). However, we note that if multiple MADDNESS matrix-vector multiplication units are used sequentially, the number of dot products required can be significantly reduced, hence improving computational speed significantly. This leads to our I/O data pruning scheme.

Furthermore, the significant volume of redundant input/output feature maps and LUT content impedes the implementation of MADDNESS on FPGA-based accelerators with limited resources. As shown in Fig.1. (c), each column of the weight matrix has a corresponding LUT with $2^I \cdot C$ cells, where I indicates the number of split indexes and C is the number of codebooks. However, not all LUTs can be used for obtaining the key information (i.e., the value on the split index) for the next layer. Therefore, the original MADDNESS algorithm executes numerous superfluous operations and generates massive amounts of redundant data that negligibly contribute to NN inference while occupying a huge volume of storage.

In order to completely decouple the time and space complexities from the input feature map resolution, and mitigate the redundancy in the generated results within layers and resource occupancy, we introduce three specific optimisation strategies: Input/output data pruning, Feature map reorganisation and Parameters compression in Section III-B1, III-B2 and III-B3 respectively, which makes AMU possible to achieve much lower latency and fewer operations for NN inference acceleration. At the same time, these optimisations also decouple the resource utilisation and Initiation Interval (II) of AMU from the problem size. In other words, by tuning the number of codebooks C and the number of prototypes 2^I for each codebook we can improve resource utilisation, accuracy and efficiency but without additional latency cost.

B. Algorithm Optimisation

We apply three design optimisation strategies to make AMU more efficient and compact: 1) Input/Output (I/O) data pruning, 2) Feature map reorganisation and 3) parameter compression, which brings two direct benefits: faster processing speed and fewer parameters for storage as shown in Fig. 2. Furthermore, they dispel the need to compute all s_j in Eq. (3), thereby eliminating the element-by-element operations in MADDNESS. This helps minimise the impact of the problem size on resource utilisation and the pipeline throughput (II) of the AMU.

1) *I/O data pruning*: In Fig. 1. (c), the original MADDNESS employs only $I \times C$ split indexes and their split values to identify prototypes from C codebooks within a given input feature map. This means that a majority of the feature

map elements remain unused for approximate matrix multiplication. Our I/O data pruning technique leverages this property to conserve FPGA resources. The I/O pruning technique retains solely the vital information including the split indexes and split values at the split indexes (e.g., coloured blocks in the codebooks as depicted in Fig. 2) prior to computing approximate matrix multiplication. In the context of inference tasks, outputting entire feature maps becomes redundant using MADDNESS since approximate matrix multiplication at the subsequent layers only requires information on split indexes to encode prototype IDs. Therefore, our pruning strategy considers the feature map structure from both the current and next approximate matrix multiplications, as all split indexes and their split values are predetermined during the offline training stage.

Now, suppose the first AMU receives an input feature map with N codebooks (each codebook has I split indexes) and the next AMU is required to receive a feature map with M codebooks (each codebook has O split indexes) as Fig. 3 (a). In the first AMU, $I \times N$ block readings are required to search optimal prototypes across N codebooks, and $O \times M$ block writings are required to write dot-product outcomes to one of O blocks across M codebooks at next AMU so that the N encoded codebooks can be used for aggregating $O \times M$ block in next AMU. The blocks in unused indexes of the input and output feature map (marked as white blocks in Fig. 2) are ignored. Due to fewer blocks required to output, the AMU only processes the approximate dot product between the input feature map and a row of weight $O \times M$ times. The associated compression ratios with a required LUT size are shown in Eq. (5) to (7).

$$\text{InputCompressionRatio}_i = \frac{I_i \cdot N_i}{U_{i-1}}, \quad (5)$$

$$\text{OutputCompressionRatio}_i = \frac{O_i \cdot M_i}{U_i}, \quad (6)$$

$$\text{LUTsize}_i = N_i \cdot 2^{I_i}, \quad (7)$$

where U_{i-1} and U_i represent the number of block readings and the number of block writings of the i -th layer using unpruned MADDNESS, respectively. Assuming the i -th layer has an input feature map ($1, U_{i-1} = 512$) and a ($U_{i-1} = 512, U_i = 512$) weight, the original MADDNESS shown in Fig. 2 need computes U_i elements for output and next layer also need read U_i elements, while this optimisation can theoretically reduce 93.75% read/write and processing operations according to Eq. (5) and (6). However, the AMU leveraging I/O data pruning with $I_i = O_i = 4$ and $N_i = M_i = 8$ in i -th layer, merely 32 blocks are received and sent.

2) *Feature map reorganisation*: I/O pruning fragments the entire feature map, dispersing valid information (i.e., the values of the split indexes) unevenly across each codebook. This fragmented feature map poses challenges for designing the high parallelism in AMUs. To overcome this issue, we restructure the pruned feature map. As shown in Fig. 3. (a), the values on the split index used in i -th encoding are assembled into the i -th package. Each package comprises N blocks from the N corresponding codebook. Additionally, the output feature map needs to be restructured to match the input

structure of the next AMU, facilitating the cascading of the AMUs to implement a dataflow-based accelerator.

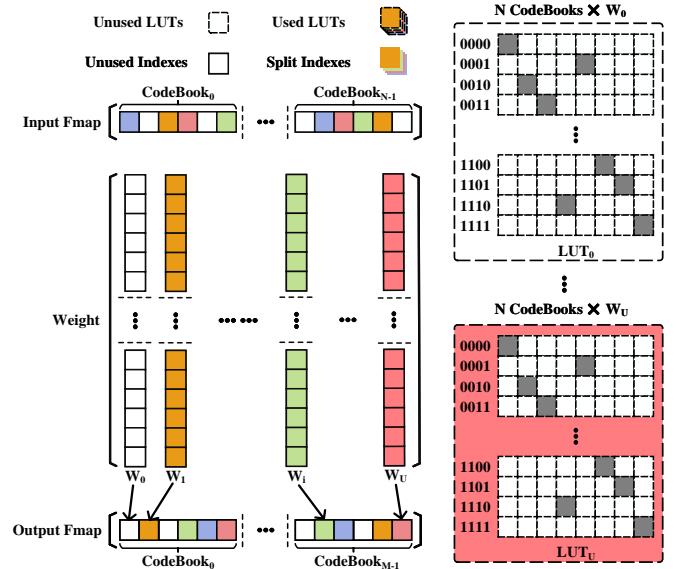


Fig. 2. I/O pruning and parameter compression: inter-layer and intra-layer redundancies can be streamlined when multiple MADDNESS matrix-vector multiplication units are used sequentially

3) *Parameters compression*: According to Fig. 2, the original MADDNESS algorithm needs to load all U LUTs for computing approximate matrix multiplication between the input feature map and U weight vectors of the weighing matrix to obtain the entire output feature map. However, because of the I/O pruning, the AMU only needs $O \times M$ LUTs, where the $O \times M \ll U$. As shown in Fig. 2, W_0 can not be used to obtain the values on the desired split indexes of the output feature map, in contrast, W_i and W_U are employed to compute the required value on split indexes of the output feature map, therefore, LUT_0 that holds the pre-computed partial dot-product of the input feature map and W_0 (i.e., N Codebooks \times W_0) is abandoned, while LUT_i and LUT_U are loaded. According to Eq. (6), for the AMU with $I_i = O_i = 4$ and $N_i = M_i = 8$ in i -th layer, and i -th layer has ($U_{i-1} = 512, U_i = 512$) weight matrix, the original MADDNESS will generate 512 LUTs, each of them owning $M \times 2^I = 128$ cells. However, only $O_i \times M_i = 32$ LUTs are required when applying parameter compression, which can reduce 93.75% of the LUTs. To parallel compute M blocks and send O package sequentially, the used LUTs are reshaped and allocated to $O \times M$ array in practice.

C. AMU Architecture Overview

AMU is based on MADDNESS architecture consisting of an allocator, encoder, and aggregator. AMU, however, optimizes each computing block according to the three proposed optimization techniques. The three processing units provide allocating blocks, finding prototypes, fetching partial results and packing the multiplication result function respectively. In the following subsections, we will introduce the three processing units respectively.

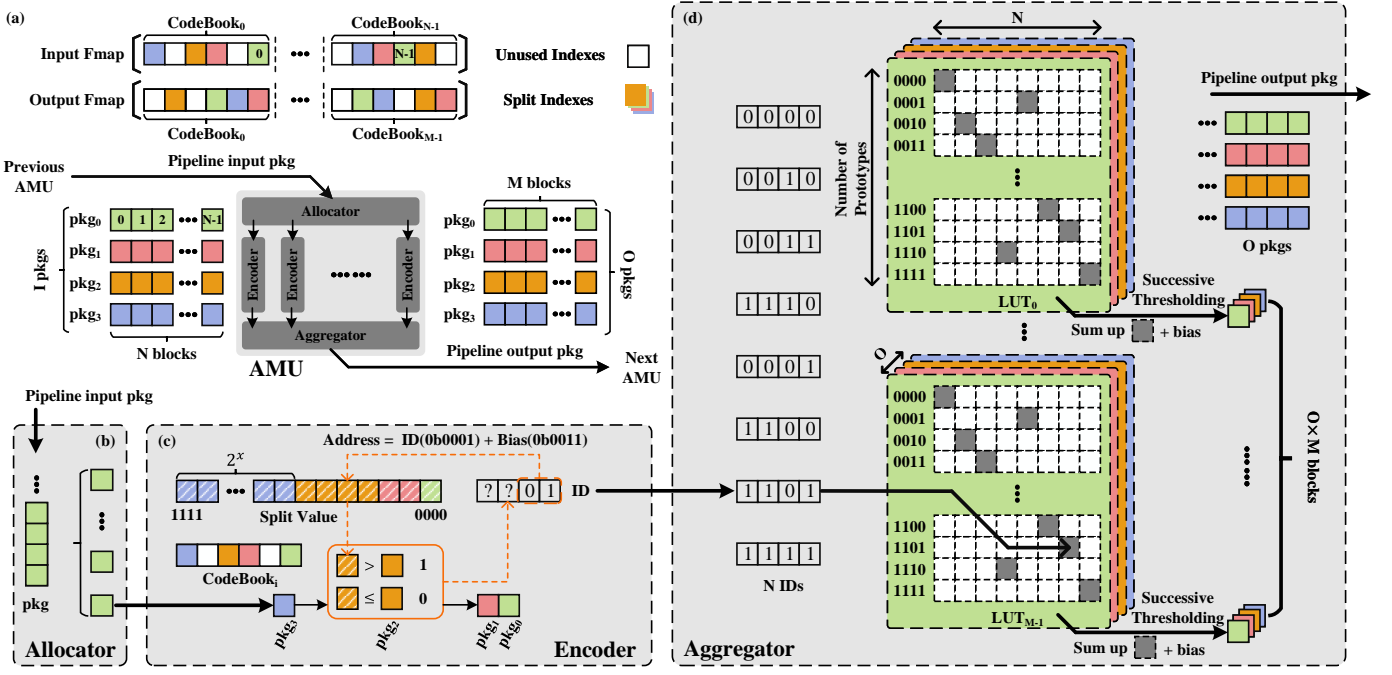


Fig. 3. Overview of the proposed AMU architecture: (a) The I/O pruning and three components of the AMU: (b) Allocator; (c) Encoder; (d) Aggregator

1) *Allocator*: Fig. 3.(a) illustrates how an AMU layer receives a pruned input feature map with $I \times N$ elements from the previous layer via I packets, where N is the number of codebooks at the input feature map, and sends O packets (each containing M blocks) as a pruned output feature map with $O \times M$ pixel to next layer, where N (or M) and I (or O) denotes that there are N (or M) codebooks in input (or output) feature map (i.e., $Fmap$) and each codebook contains I (or O) split indexes. The main function of the allocator is to unpack the received package and allocate them to N parallel encoders. As shown in Fig. 3.(b), due to feature map reorganisation in Section III-B2, $I \times Q \times N$ -bits-packages (i.e., a pkg) will be arrived successively. For each package, the allocator employs a bitwise operator to take out $N \times Q$ -bits-values (i.e., N blocks). Here Q determines the quantisation level of activation or weight in the inference networks.

2) *Encoder*: The N blocks are unpacked to N corresponding encoders, each encoder is assigned to encode the ID of a certain codebook (e.g. $CodeBook_i$), which is used to look up the dot product result of the corresponding prototype as well as the weight sub-matrix in the aggregator. As shown in Fig. 3.(c), the encoder reads blocks serially, for each round, the encoder takes the current block from the input package and the corresponding split value to identify the next round ID. Here the $2^I - 1$ split values are allocated to a sequential array. In the j^{th} round the split value on $Address = ID_{j-1} + Bias$ is taken to compare with the current block, where ID_{j-1} indicates the last round ID and $Bias = 2^j - 1$. Once the encoder has processed all blocks, it can obtain an ID indicating the prototype address of $CodeBook_i$.

3) *Aggregator*: In Fig. 3.(d), the $N = 8$, $I = 4$ and $O = 4$ case is demonstrated. The aggregator is on standby until all IDs are ready. For each $CodeBook$, there is a distinct prototype

ID ranging from $0b0000$ to $0b1111$ (2^I prototypes in total). Consider the ID 1101 is the prototype address of the 7th codebook (i.e., $CodeBook_6$), the cells on all LUTs located in (13, 6) are picked as the partial dot product result of the input feature map and weight. All picked cells (marked as grey cells) are summed up and bias is added if required. They are then passed through successive thresholding (i.e., a quantised NN operator, equivalent to scaling, batch normalisation, and uniform-quantised activation) [20] to obtain $O \times M$ blocks and pipelined to send O packages to the next AMU. The aggregator contains $O \times M$ LUTs obtained from the offline training stage, each LUT has $I \times N$ approximate partial product results. By tuning O/I and M/N we can scale the LUT of the aggregator to achieve the desired resource-efficiency-accuracy for the AMU-based NN inference acceleration.

D. Hardware Design Space Exploration

Unlike GEMM using element-by-element arithmetic operations, the AMU uses unstructured pruning and utilises atypical memory accesses to achieve matrix multiplications. The sparse matrices derived from the pruning result in atypical memory access behaviour, posing an additional challenge for designing efficient accelerators. As shown in Fig. 3, the main memory accesses occur in the encoding and aggregating stage. Meanwhile, to store the partial dot-product of all prototypes and weight matrix, the LUT can largely occupy the main memory resource. Therefore, the memory allocation of LUTs and the design of aggregator memory accesses are essential to improve the resource utilisation and throughput of AMUs.

1) *Memory allocation design*: To properly leverage the storage resources of the device, we analysed the array structure of the LUT. As depicted in Fig. 4, each codebook can only be identified as a specific prototype, requiring only one partial

dot product to be read from each column to compute a single pixel of the output feature map (i.e., there is only one grey cell in each column of the LUT). Based on this feature, we allocate the LUTs to various dual-port ROMs (termed as ‘Group’ partition), each containing every $2 \times S \times O \times E$ -columns partial dot product from LUTs, where $S \in \{1, 2, 3, \dots, \lfloor N/2 \rfloor\}$ and $E \in \{1, 2, 3, \dots, M\}$. For example, an AMU with N input codebooks and M output codebooks can be assigned $M \times N/S \times E$ dual-port ROM. While larger S or E enhances memory utilisation by minimizing unused regions in each ROM, it incurs $\alpha \times O \times S \times E$ latency in fetching all dot product results from a dual-port ROM. Here, we suppose α is the average clock cycle delay of an operation in Fig. 4.

2) *Memory accesses pipeline design*: From the other perspective, the throughput is always desired for designing an efficient accelerator. A well-designed memory access architecture can provide the promised II and consequently can significantly improve the throughput of the AMU. As shown in Fig. 4, the II of the AMU is the time delay in cycles, between the launch of processing successive input feature maps. Two crucial bottlenecks prevent AMUs from achieving lower II (i.e., the red double arrows in Fig. 4). Specifically, (1) sequentially allocating and encoding packages results in $\alpha \times I$ clock cycle delay, and (2) aggregating partial dot product from $\alpha \times M \times N/S \times E$ dual-port ROM results in $\alpha \times S \times E$ clock cycle delay. The final II of the AMU is the maximum delay between two bottlenecks.

To address the bottleneck of (1), where data dependencies exist not only between allocating and encoding packages but also between encoding packages of an input feature map, we can assemble all packages and transmit them within a single operation. This enables the encoder to process successive input feature maps in a pipeline. For the bottleneck of (2), caused by dual-port ROM read blocking, there is $\alpha \times O \times S \times E$ clock cycle delay between two successive input feature maps. To compress this delay, we can decrease S or E . In an extreme scenario, we can allocate every column or even every cell of LUTs to distributed ROMs or separated registers (termed as ‘Complete’ partition) so that all the grey cells can be fetched at once without read conflicts, which enables fully unroll aggregating processes to achieve the best throughput.

E. AMU-based QNN accelerator

1) *Design Principles*: Based on the study from the [19], it was found that the accuracy of a model decreases as more layers are replaced by approximate matrix multiplication as in MADDNESS [15] and Vanilla PQ-based multiplication [19]. The accumulating errors through these approximate multiplications are difficult to eliminate. Even when using a differentiable implementation as shown in Halutmatmul [18], the accuracy of Halutmatmul-based NN decreases statistically as the network gets deeper. However, both authors [19], [18] found that using exact matrix multiplication for the first hidden layer results in a considerable accuracy gain in accuracy for the NN model that uses approximate matrix multiplication. For clarification, we use the term “exact matrix multiplication” for the matrix multiplication using single precision arithmetic (i.e., 32-bit floating point arithmetic) in the paper. Thus, the

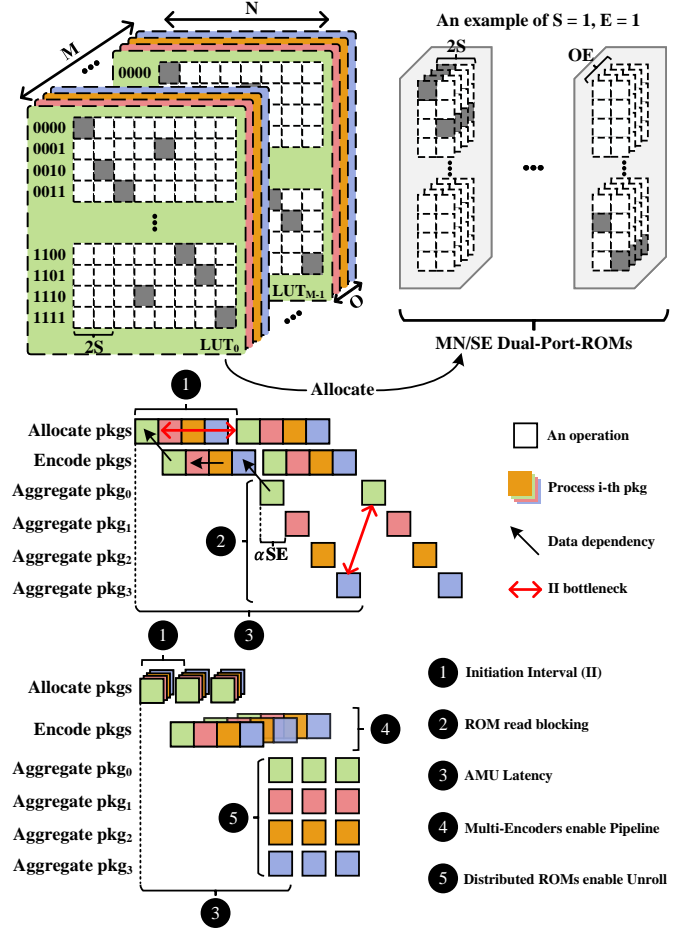


Fig. 4. AMU resource utilisation and throughput (II) analysis

configuration of the first layer in the AMU-based NN can greatly impact the accuracy of the NN inference.

To quantify the impact of the first hidden layer configuration on the accuracy of the AMU-based NN inference, we investigate the degradation of accuracy with increasing NN depth for different first-hidden layer settings of AMU-based MLP on the MNIST dataset. The MLP contains repeated hidden layers (a hidden layer includes: 256×256 linear transfer, batch normalization, activation, and dropout) and a classification layer (256×10 linear transfer). As shown in the left part of Fig. 5, all hidden and classification layers are replaced into ($I = 4, N = 16$) AMU, except the first hidden layer with 4 different settings: using more codebooks ($I = 4, N = 32$), more prototypes ($I = 5, N = 32$), exact matrix multiplication (the up boundary of the AMU when $N = 28 \times 28, I \rightarrow \infty$) and default AMU ($N = 16, I = 4$).

The AMU-based MLP using exact matrix multiplication for the first hidden layer shows the best accuracy, compared to the other AMUs. The AMU with larger LUT (based on Eq. (7)) exhibits superior accuracy. For example, Fig. 5 shows the accuracy ranges: 74.6% - 65.4% for $I = 5, N = 16$ vs 69.1% - 58.8% $I = 4, N = 16$ and 78.5% - 70.5% for $I = 4, N = 32$ vs 69.1% - 58.8% for $I = 4, N = 16$. Additionally, given a LUT size budget, using more codebooks (78.5% - 70.5% for $I = 4, N = 32, \text{LUT size} = 16 \times 32$ items) can own better accuracy

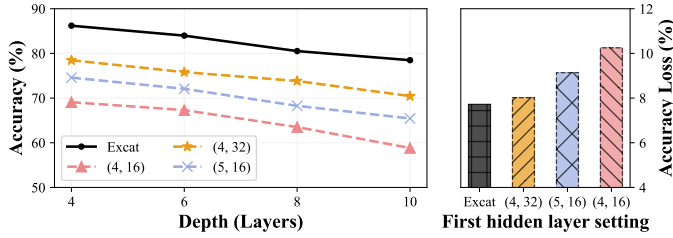


Fig. 5. The impact of prefix layer configurations on AMU-based MLP accuracy as depth increases, using the first layer setting as an example. “Exact” is ‘Exact matrix multiplication’, the pair (I, N) represent I codebooks and N prototypes for the first hidden layer (The rest layers with setting $(4, 16)$)

compared with using more prototypes (74.6% - 65.4% for $I = 5, N = 16$, LUT size = 32×16 items). In our experimental setup, using more codebooks in the first hidden layer can provide better accuracy and a better effect on alleviating accuracy loss with increasing depth of NN, compared to using more prototypes. Similarly, to further raise the upper bound of accuracy (i.e., the black line in Fig. 5), increasing the number of codebooks in the subsequent layer is required. This suggests that given an LUT budget, there would be an optimal value for I and N according to the data and NN structure. For example, cross-validation approach [28] can be effectively used to seek the optimal I and N to further optimize the AMU - this paper focuses on AMU design (i.e., how to optimize MADDNESS for FPGAs using the three optimization techniques).

As another noticeable observation, as the depth of the NN is increased from 4 layers to 10 layers, using the exact matrix multiplication at the first hidden layer experiences less accuracy loss (7.7%), compared to the baseline setting using $I = 4, N = 16$ AMU (10.2%) in Fig. 5, even though the exact matrix multiplication setting starts with a higher accuracy.

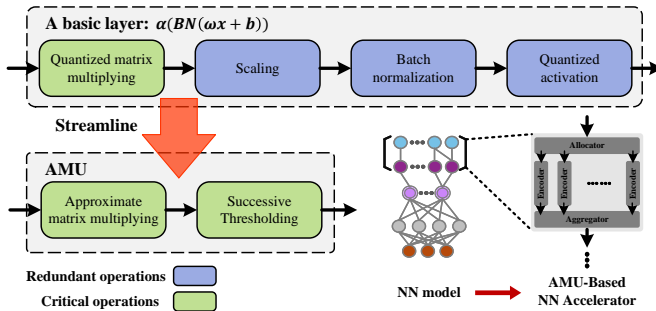


Fig. 6. Using FINN pipeline [10] to streamline basic layers for the AMU-based NN accelerator

2) *Deploying accelerator*: To deploy the AMU-based NN accelerator, we employed the FINN pipeline as a development tool. FINN is an FPGA-oriented, streamlined QNNS and end-to-end deployment tool. It can automatically generate a customized FPGA-based accelerator for a quantized inference network. The key techniques of FINN can be summarised as two compression strategies: streamline and folding strategies, which make FINN possible to transform an abstract inference network into a topological map cascaded by a series of reusable basic logic units for QNN accelerator: Sliding Win-

dows Unit, Pool Unit, and MVAU. The topological map is then converted into a synchronous dataflow model by assembling basic computation units to corresponding independent modules and inserting dataflow-supported buffers. Finally, a QNN is mapped into an FPGA accelerator.

As shown in Fig. 6, we leverage the streamline strategy to eliminate the redundant operations of the basic layer: scaling, batch normalisation, and activation operation, and substitute them with successive thresholding operations. By streamlining the operations, the AMU can compute $\alpha(BN(wx+b))$ simply using approximate matrix multiplication and successive thresholding operations. The convolution operation can be treated as a series of matrix multiplication by leveraging the `img2col` or `kn2col` function. Finally, an NN model can be then converted into an FPGA-based accelerator with cascaded AMU kernels.

IV. EVALUATION

To evaluate the performance of the proposed AMU, we implement the AMU module on a Xilinx ZCU104 platform with regards of the following four design perspectives: 1) exploring the optimal hardware setting for the best throughput and energy efficiency trade-off for a single AMU module; 2) evaluating the single AMU performance in NN inference tasks with various problem sizes; 3) investigating the performance of AMU-based NN accelerator against different optimisation strategies; 4) comparing the performance of the AMU-based NN accelerator with the prior works.

A. Hardware Resources Assessments

TABLE I
AMU V.S MVAU IMPLEMENTATIONS ON ZCU104@100 MHz WITH DIFFERENT MEMORY ALLOCATION & ACCESS DESIGN

	LUT/Weight Shape ¹	Resource			Efficiency ² (GOPS/W)
		LUT	FF	BRAM	
AMU	(8, 16)	1908	262	0	92.8
	(4, 16)	2490	480	0	180.7
	(2, 16)	2821	600	0	345.3
	(1, 16)	2859	734	0	634.9
	Complete	5061	3067	0	23518.9
MVAU [11]	(16, 16)	836	616	0	89.1
	(16, 32)	1651	797	16	170.4
	(32, 32)	3080	1023	32	317.2
	(32, 64)	4925	1149	64	557.6
	(128, 128)	27418	2478	0	2072.8

¹ LUT shape for AMU: ‘Group’ partition split factor (S, E) or ‘Complete’ partition in section III-D; Weight shape for MVAU: (PE, SIMD).

² Efficiency = Throughput/(PL Static Power + PL Dynamic Power)

To explore the memory allocation and access design for achieving the best throughput and energy efficiency of the single AMU module, we evaluate 5 different LUT configurations as illustrated in Table I. According to Table I, both MVAU and AMU only need on-chip memory (i.e., BRAM or LUT) to store the quantised parameters for small-scale NN models, so their performance is not subject to data movement overhead of external memory access. As discussed in Section III-D, the

LUTs can be allocated every $2 \times S \times O \times E$ -columns as a block to each Dual-port-ROMs, where the S and E indicates split factor ranged from $S \in \{1, \dots, \lfloor N/2 \rfloor\}$ and $E \in \{1, \dots, M\}$, respectively. However, in an extreme scenario, LUTs can be completely partitioned as distributed ROMs to achieve the best throughput (i.e., using the ‘Complete’ partition introduced in Section III-D2). Additionally, 5 different MVAUs with varying weight matrix shapes were quoted as a baseline, each with different PE and $SIMD$, indicating the parallelism level of MVAU. We evaluate the throughput (i.e., FPS) of the MVAU based on Eq. (8), where F_{clk} is the device clock frequency, and F is the total fold defined in Eq. (9) [10].

$$FPS = F_{clk}/F = F_{clk}/II \quad (8)$$

$$F = MatrixH/SIMD \cdot MatrixW/PE \quad (9)$$

All modules are tested on the same problem size (i.e., (256, 256) weight matrix or 0.13 MOPs), and the AMUs have the same hyper-parameter $I = 4$, $N = 16$, $O = 4$, and $M = 8$. As shown in Fig. 7, the AMU with ‘Group’ partition (8, 16), (4, 16), (2, 16) and (1, 16) has a similar II as the MVAU with (16, 16), (16, 32), (32, 32) and (32, 64), respectively, while has 20 - 61 mW lower power consumption due to utilizing less resource (according to Table I). Additionally, the AMU with a ‘Complete’ partition consuming 75 mW lower power consumption achieves $II = 1$, compared with the MVAU with ($PE = 128$, $SIMD = 128$), which fails to break through the practical boundary $II = 10$ to reach the theoretical $II = 4$ at $F = 4$. From another perspective, Table I indicates that the AMU with the ‘Complete’ partition achieves significant gains in energy efficiency, which is $37\times$ and $11.3\times$ over the AMU with the ‘Group’ partition ($S = 1$, $E = 16$), and the MVAU with ($PE = 128$, $SIMD = 128$), respectively. However, the ‘Complete’ partition incurs 1.8 to $2.7\times$ LUT resource occupancy, compared with other partition strategies.

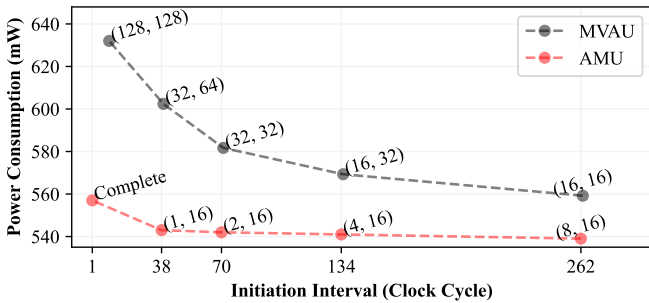


Fig. 7. Pareto Optimal of the AMU and MVAU on ZCU104 with clock frequency at 100 MHz

The analysis of Table I and Fig. 7, suggest that the AMU forsakes the elements-wise arithmetic operation, which can obtain significant improvements in energy efficiency, compared to the MVAU [11], by aiding with suitable memory allocation and memory access design for the atypical logic behaviours (i.e., the operation in three components of AMU: Allocator, Encoder and Aggregator) derived from unstructured pruning (i.e., three optimisations: I/O data pruning, feature map reorganisation and parameters compression). Moreover,

the unbeatable II of the AMU module using complete partition permits the AMU-based NN accelerator to achieve stunning throughput.

B. Single AMU performance on various problem sizes

To investigate the effect of various problem sizes on a single AMU performance in the context of the NN inference, we replace the classification layer (i.e., MVAU module) of the FINN-generated [10] 1-bit precision TFC, SFC and CNV accelerator to AMU, and restructure the input activation as an available input package for AMU to emulate the single unit on an AMU-based accelerator. Here, CNV refers to an image classification network designed for CIFAR-10, featuring a (512, 10) weight matrix in its classification layer. Meanwhile, TFC and SFC are networks tailored for handwriting number classification on the MNIST dataset, with weight matrices of (64, 10) and (256, 10), respectively. The input activation is captured from the interval output of the FINN-generated accelerators.

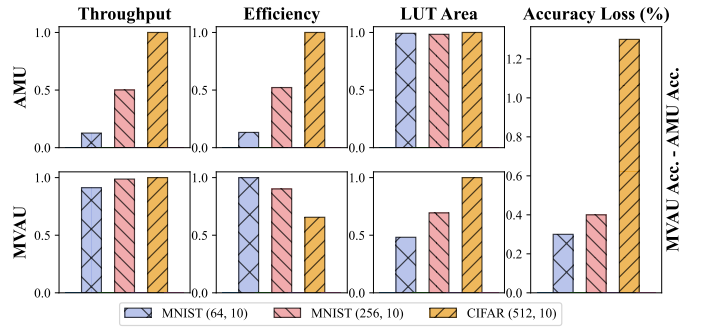


Fig. 8. The impact of problem sizes for the performance of the MVAU/AMU classification layer (i.e., normalised throughput, efficiency and LUT area) on ZCU104 platform@100 MHz. AMU settings: $I = 4$, $N = 8$, $M = 1$ and $O = 10$, MVAU settings: $SIMD = 8$ and $PE = 1$

The FINN [10] introduced the hyper-parameters $SIMD$ and PE for MVAU, which are the number of input data parallelism and the number of processing element, respectively. As the last fully connected layer, the MVAU needs $SIMD \times Y$ bit-width input package, while the AMU requires $N \times Y$ bit-width input package, and both matrix multipliers need output 10 16-bit values for the final soft-max operation. Here Y suggests the input packages quantised level, $SIMD$ is the read parallelism level in MVAU and N is the number of codebooks for an input feature map in AMU. In this experiment, we assign $I = 4$, $N = 8$, $M = 1$ and $O = 10$ AMU, and $SIMD = 8$ and $PE = 1$ MVAU (FINN default folding parameters) for both classification layers.

Fig. 8 illustrates the relative performance change of the MVAU/AMU classification layer across various problem sizes (i.e., the weight matrix size). The performances of each implementation are measured in terms of throughput, efficiency, LUT area, and classification accuracy. To compare the relative performance change, the sub-figures of the throughput, efficiency, and LUT area columns are normalized by their maximum values. For the accuracy loss, the MVAU-based NN accelerator’s classification accuracy serves as the baseline, which is defined as the accuracy of the MVAU-based

classification layer subtracting the accuracy of the AMU-based classification layer. As the problem size increases from MNIST (64, 10) to CIFAR10 (512, 10), the AMU-based classification layer significantly increases $4\times$ in terms of throughput and energy efficiency at the same level of LUT utilisation, while introduces 1.2% accuracy loss. However, the MVAU-based classification layer only earns $1.1\times$ throughput improvement, while it drops 40% in energy efficiency with $2\times$ LUT area utilisation. This implies that AMUs attain optimal throughput and energy efficiency within available resources, such as LUTs, while maintaining accuracy balance.

The analysis of Fig. 8 reveals that the MVAU, a typical element-wise arithmetic-based matrix multiplier, suffers from the growing resource costs and throughput bottleneck along with the larger problem size, thereby resulting in efficiency degradation in MVAU. This is because the elements-wise arithmetic operation-based matrix multiplier can only process restricted operations within the same parallelism level. On the contrary, the AMU eliminates the element-wise arithmetic operations, which own a proportional gain on the throughput and energy efficiency while maintaining consistent resource cost (i.e., LUT utilisation) along with increasing the problem sizes (i.e., the weight matrix size). This is because AMU with pruning optimisation always needs to process the identical input information volume and send the same output information volume once I , N , O , and M are decided. However, using the same hyper-parameters for the larger problem size and more complex classification task inevitably results in a loss of accuracy due to insufficient codebooks and prototypes for describing the more sophisticated feature distribution. To address the prediction accuracy loss, the most effective way is increasing the number of the codebooks in the first hidden layer as discussed in Section III-E1.

C. AMU-based accelerators performance in different settings

TABLE II
RESOURCE UTILISATION OF THE SFC IMPLEMENTATIONS ON ZCU104

Computation Unit	Hyper ¹ Parameters	Resource Utilization		
		LUT	FF	DSP
AMUNet-0	(3, 64), (3, 32), (3, 16), (3, 8)	72504	31846	0
AMUNet-1	(4, 64), (4, 32), (4, 16), (4, 8)	128265	69874	0
AMUNet-2	(4, 72), (4, 36), (4, 36), (4, 18)	193955	119629	0
MVAU[11]	(392, 128), (128, 128), (128, 128), (128, 10)	132544	14943	0
LUTNet[29]	(4, 0)	96571	47175	1532

¹ (SIMD, PE) for MVAU, (K, P) for LUTNet and (I, N) for AMU.

To investigate the performance of the AMU-based accelerator under the different optimisation strategies, we employ the 1-bit quantised SFC as a target NN. The SFC is constructed by 4 successive fully connected layers, each of them has (784, 256), (256, 256), (256, 256) and (256, 10) weight matrix. As illustrated in Table II, we design and implement 3 different AMU-based NN accelerators targeted for high-efficiency, balance, and high-accuracy optimisations:

- **AMUNet-0**: to achieve high efficiency, we assign fewer prototypes (i.e., $I_i = 3$, where $i \in [0, 3]$ and $N_0 = 64$,

$N_1 = 32$, $N_2 = 16$ and $N_3 = 8$) for each layer to restrict the power consumption.

- **AMUNet-1**: to achieve balanced accuracy and efficiency, we assign regular prototype numbers and codebook numbers (i.e., $I_i = 4$, where $i \in [0, 3]$ and $N_0 = 64$, $N_1 = 32$, $N_2 = 16$ and $N_3 = 8$) for each layer to strike a balance between accuracy and efficiency performance.
- **AMUNet-2**: to achieve high accuracy, we assign more codebooks (i.e., $I_i = 4$, where $i \in [0, 3]$ and $N_0 = 72$, $N_1 = 36$, $N_2 = 36$ and $N_3 = 18$) for each layer to improve the accuracy.

The number of output package O_i and the number of blocks in each output package M_i is the same as I_{i+1} and N_{i+1} , where $i \leq 2$ represents the i^{th} AMU in the NN accelerator. All AMU units in three accelerators apply the ‘Complete’ partition and all accelerators will generate $O_3 = 10$ output package and each output package has $M = 1$ block (i.e., 10 16-bit values for final soft-max operation). In addition, a FINN-generated MVAU-based accelerator [10] and a LUTNet-based SFC accelerator [29] are implemented as the baseline:

- **MVAU-based NN accelerator (MVAU)**: this accelerator has $SIMD_0 = 392$, $SIMD_i = 128$, $i \in [1, 3]$, and $PE_i = 128$, $i \in [0, 2]$, $PE_3 = 5$. The total fold $F = 4$ according to Eq. (9) for each layer i . Theoretically, it will have the same level throughput $FPS = 2 \times 10^7$ (according to Eq. 8) as an AMU-based accelerator when the clock frequency $F_{clk} = 100$ MHz.
- **Unrolled LUTNet (LUTNet)**: this accelerator has $K = 4$ and $P = 0$, where K indicates the accelerator can perform an arbitrary Boolean operation on up to 4 inputs, and $P = 0$ means unrolled architecture [29].

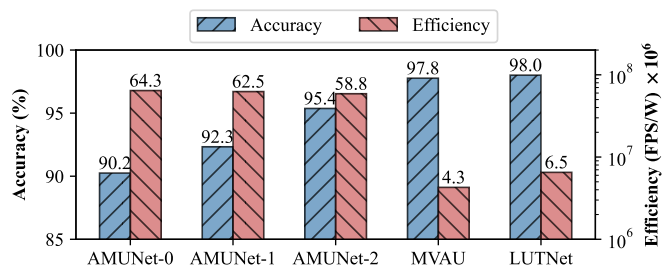


Fig. 9. Efficiency and MNIST dataset classification Accuracy comparison of SFC accelerators on ZCU104 @ 100 MHz

All accelerators are tested on a ZCU104 board with the clock frequency 100 MHz. As shown in Fig. 9 and Table II, with increasing the LUTs utilisation, the AMU-based accelerator gains 5.2% accuracy improvement. However, the growth in resource occupancy introduces more power consumption, resulting in a 5.5×10^6 FPS/W drop in efficiency from AMUNet-0 to AMUNet-2. The comparison among AMU-based NN accelerators reveals that adjusting the hyper-parameters I and N for each AMU enables us to achieve diverse efficiency-accuracy trade-offs. This capability enables the AMU to achieve superior efficiency while maintaining acceptable accuracy or to attain higher accuracy within the constraints of the available LUT resources. For example, the

TABLE III
THROUGHPUT AND EFFICIENCY COMPARISON OF AMU-BASED ACCELERATOR IMPLEMENTATION AND PREVIOUS WORK

	Platform	Precision	Model Structure	Parameter Size (M)	Complexity (MOPs)	Frequency (MHz)	Throughput (GOPS)	Efficiency (GOPS/W)	Resource Utilization			
									LUT	BRAM	FF	DSP
Our work ¹	ZCU104	FIX8	SFC	0.12	0.6	100	66,999	39,411	193,955	-	119,629	-
	XCZU19EG	FIX8	CNV	0.06	57.8	100	7,372	6,456	39,588	-	21,197	-
	XCZU19EG	FIX8	CNV	0.2	79.4	100	9,913	8,039	120,835	-	73,557	-
	XCZU19EG	FIX8	CNV	0.46	109.0	100	13,608	8,906	198,923	-	118,187	-
FINN [10]	ZC706	INT1	SFC	0.3	0.6	200	7,416	350	91,131	4.5@36k	-	-
	Ultra96	INT1	CNV	1.5	115.8	300	2,318	217	41,733	283@18k	-	-
TCS II'20 [30]	VC707	FIX18	Shufflenet	-	137.0	200	108	12	198,129	1,027@32k	117,091	1,926
Angel-Eye [23]	XC7Z045	FIX16	-	-	552.0	150	137	14	182,616	486@36k	127,653	780
DNNBuilder [24]	ZC7Z045	FIX8	AlexNet	61	2900.0	200	494	47	86,262	303@36k	51,378	808
Stella Nera ² [18]	ASIC	INT8	Resnet-9	2.44	574.2	624	2,900	43,100	-	-	-	-

¹ The AMU-based NN accelerator processes binary feature maps with the 8-bit precision LUT.

² The Stella Nera processes FP16 inputs and outputs with the 8-bit precision LUT.

AMUNet-2 achieves $9.1\times$ and $13.7\times$ efficiency over LUTNet and MVAU within the same level resource cost, while introducing $\leq 2.6\%$ accuracy loss. This observation indicates that forsaking element-by-element arithmetic operations release the potential of the AMU-based NN accelerator for achieving significant gains in efficiency, compared with the traditional element-wise arithmetic-based matrix multipliers.

D. Performance comparison

To validate the performance of the proposed AMU module in the context of NN inference acceleration, we implemented AMU-based NN accelerators for the SFC model (i.e., a four-layer MLP for MNIST) and convolution layers of CNV model (i.e a VGG inspired CNN for CIFAR10) on ZCU104 and XCZU19EG respectively, together with 7 prior works implemented on different platforms with varying frequencies and validated by different task complexities (i.e., the total computing operations of the neural network). In order to make AMU compatible with convolution computation, the convolution operations are transformed into a series of matrix multiplications by using the `img2col` function. We substituted three successive convolution layers in the CNV model progressively, which takes 50%, 69% and 94% of total computational cost (i.e., 57.8, 79.4 and 109 MOPs), with AMUs to illustrate the AMU-based accelerator performance when it encountering with the convolution operation. As shown in Table III, the peak throughput and peak efficiency are recorded as the key criteria for demonstrating the performance of each accelerator in this table. The resource utilization of each accelerator is measured by the volumes of LUT, BRAM, FF, and DSP utilisation.

As illustrated in Table III, the proposed work, AMU-based NN accelerator, for the SFC (0.6 MOPs) at 100 MHz outperforms MVAU-based [10] NN accelerators at 200 MHz by $9\times$ in throughput and $112\times$ in energy efficiency, while introducing $2.1\times$ LUT occupancy. However, the growing complexity of convolution NNs (from 57.8 MOPs to 79.4 MOPs) introduces a $1.4\times$ throughput of the AMU-based NN accelerator, which also results in $3\times$ LUT and $3.5\times$ Flip Flop occupancy because of increasing demands for larger parameter storage and maintaining high throughput. To cope with

resource shortage, the AMU-based NN accelerator applies a ‘Group’ partition strategy for the 109 MOPs CNV convolution layers, achieving 3×10^5 and 1.7×10^5 per million parameter growth in LUT and FF occupancy. Less than 5.8×10^6 and 3.7×10^6 per million parameter growth in LUT and FF occupancy compared with the other two CNV implementations using the ‘Complete’ partition strategy. As shown in Table III, with growth in CNV model complexity and parameter size, the AMU-based accelerators own increasing throughput and energy efficiency, which indicates that the proposed work has attractive scalability.

From another perspective, AMU-based NN accelerators for the CNV convolution layers achieve higher energy efficiency, ranged from 6456 GOPS/W to 8906 GOPS/W. This surpasses state-of-the-art NN accelerators including FINN (MVAU-based accelerator) [10], Angel-Eye [23], DNNBuilder [24] and TCS II'20 [30]. Angel-Eye and DNNBuilder are FPGA-oriented End-to-End CNN deployment frameworks, while the TCS II'20 proposed a general solution for accelerating matrix-matrix multiplication on FPGA [30]. Those works are validated on a face recognition CNN model (552 MOPs), Alexnet (2900 MOPs) and Shufflenet (137 MOPs), respectively. Although the complexity and parameter size of our works are different from these works which results in different throughput and resource utilization, the proposed memory allocation and access strategies suggest that the AMU-based accelerator has better scalability, which can potentially achieve better energy efficiency at a higher level of complexity.

In addition, our method achieved $4.7\times$ throughput to Stella Nera [18] in a similar level of complexities (from 109 MOPs to 574.16 MOPs), where the Stella Nera using Halutmatmul, a matrix multiplication method based on MADDNESS, is an ASIC-based accelerator (14 nm) for Resnet-9. Our work owning a comparable performance to ASIC-based accelerator indicates that the proposed three optimization strategies and dedicated hardware design for atypical memory allocation and access are capable of facilitating MADDNESS-based matrix multiplication to achieve better performance on ASIC-based accelerators.

The analysis of Table III suggests that eliminating element-

wise arithmetic operation together with software-hardware co-design optimisation for atypical logic behaviours releases the potential of the AMU-based NN accelerator, achieving significant gains in throughput (up to $9\times$) and energy efficiency (up to $112\times$), compared to the accelerator using element-wise arithmetic-based matrix multipliers in the same complexity inference task.

V. CONCLUSION

In this paper, we proposed a novel approximate multiplier unit: AMU, a scalable, energy-efficient and element-wise arithmetic operation-free matrix multiplication unit that aims to build fast, and efficient dataflow-type accelerators for the quantised NNs on FPGA. Furthermore, by replacing element-by-element arithmetic operation with encoding, retrieval and summation, the proposed AMU-based dataflow-type accelerator achieves $9\times$ throughput and $112\times$ energy efficiency than FINN-generated MVAU-based accelerator that uses bit-wise and pop-count operation on the quantised elements for the NN inference task with the same complexity level, while sacrificing acceptable accuracy loss and resource burden. The pruning and compression optimisation for the MADDNESS algorithm together with dedicated memory allocation and memory access design for FPGA enables our approach to achieve competitive performance compared to an ASIC accelerator using the original MADNESS-based matrix multiplication. However, the original MADNESS introduces an inevitable accuracy loss in an AMU-based accelerator, and this issue arises from the clustering strategy used in the approximate matrix multiplication algorithm, where each AMU is only responsible for its output and disregards its connection to the final network inference results. Additionally, our studies thus suggest that instead of increasing I and N for every layer, using more codebooks in the first few hidden layers can provide better accuracy and better effect on alleviating accuracy loss with increasing depth of NN, while introducing less resource cost. However, the proposed pruning and compression optimisation for MADDNESS algorithm may degrade performance when encountering complex NNs, especially for the NNs that have a convolution layer, encouraging us to explore the effective optimisation for those commonly appeared operations in deeper NNs for future work.

ACKNOWLEDGMENT

This work is supported by the UK Engineering and Physical Sciences Research Council through grants, EP/X015955/1, EP/X019160/1 and EP/V000462/1, EP/V034111/1. For the purpose of open access, the author has applied a Creative Commons Attribution (CC BY) licence to any Author Accepted Manuscript version arising.

REFERENCES

- [1] Y. Hu, Y. Liu, and Z. Liu, "A survey on convolutional neural network accelerators: Gpu, fpga and asic," *2022 ICCRD 2022*, pp. 100–107, 2022.
- [2] C. Gao *et al.*, "Application level resource scheduling for deep learning acceleration on mpsoe," *Journal of Signal Processing Systems*, vol. 95, no. 10, pp. 1231–1243, 2023.

- [3] X. Zhu *et al.*, "Bayesian optimization for efficient heterogeneous mpsoe based dnn accelerator runtime tuning," in *2023 FPL*, 2023, pp. 355–356.
- [4] C. Gao *et al.*, "Modelling and analysis of fpga-based mpsoe system with multiple dnn accelerators," in *2023 21st IEEE NEWCAS*, 2023, pp. 1–5.
- [5] A. Rahim *et al.*, "Enhancing smart home security: Anomaly detection and face recognition in smart home iot devices using logit-boosted cnn models," *Sensors*, vol. 23, no. 15, p. 6979, 2023.
- [6] S. A. Peixoto *et al.*, "A high-efficiency energy and storage approach for iot applications of facial recognition," *Image and Vision Computing*, vol. 96, p. 103899, 2020.
- [7] M. Straczekiewicz, P. James, and J.-P. Onnela, "A systematic review of smartphone-based human activity recognition for health research," *arXiv preprint arXiv:1910.03970*, 2019.
- [8] J. Lee *et al.*, "Resource-efficient convolutional networks: A survey on model-, arithmetic-, and implementation-level techniques," *ACM Comput. Surv.*, vol. 55, no. 13s, jul 2023.
- [9] S. Liang, S. Yin, L. Liu, W. Luk, and S. Wei, "Fp-bnn: Binarized neural network on fpga," *Neurocomputing*, vol. 275, pp. 1072–1086, 1 2018.
- [10] M. Blott *et al.*, "Finn-r: An end-to-end deep-learning framework for fast exploration of quantized neural networks," *ACM TRTS*, vol. 11, 2018.
- [11] Y. Umuroglu and N. J. Fraser, "Finn: A framework for fast, scalable binarized neural network inference," *FPGA 2017*, pp. 65–74, 2017.
- [12] F. Hamanaka, T. Odan, K. Kise, and T. V. Chu, "An exploration of state-of-the-art automation frameworks for fpga-based dnn acceleration," *IEEE Access*, vol. 11, pp. 5701–5713, 2023.
- [13] E. Wang *et al.*, "Lutnet: Learning fpga configurations for highly efficient neural network inference," *IEEE Transactions on Computers*, vol. 69, pp. 1795–1808, 2020.
- [14] Y. Zhang and J. Pan, "Fracbnn: Accurate and fpga-efficient binary neural networks with fractional activations," *FPGA 2021*, pp. 171–182, 2021.
- [15] D. Blalock and J. Gutttag, "Multiplying matrices without multiplying," in *ICML*. PMLR, 2021, pp. 992–1004.
- [16] H. Jégou, M. Douze, and C. Schmid, "Product quantization for nearest neighbor search," *IEEE TPAMI*, vol. 33, no. 1, pp. 117–128, Jan 2011.
- [17] R. Guo, S. Kumar, K. Choromanski, and D. Simcha, "Quantization based fast inner product search," in *Artificial intelligence and statistics*. PMLR, 2016, pp. 482–490.
- [18] J. Schönleber, *et al.*, "Stella nera: Achieving 161 top/s/w with multiplier-free dnn acceleration based on approximate matrix multiplication," *arXiv preprint arXiv:2311.10207*, 2023.
- [19] X. Tang, *et al.*, "Lut-nn: Empower efficient neural network inference with centroid learning and table lookup," in *Proceedings of the 29th MobiCom*, 2023, pp. 1–15.
- [20] Y. Umuroglu and M. Jahre, "Streamlined deployment for quantized neural networks," *arXiv preprint arXiv:1709.04060*, 2017.
- [21] T. Aarrestad *et al.*, "Fast convolutional neural networks on fpgas with hls4ml," 1 2021.
- [22] S. Basalama *et al.*, "Flexcnn: An end-to-end framework for composing cnn accelerators on fpga," *ACM Trans. Reconfigurable Technol. Syst.*, vol. 16, no. 2, mar 2023.
- [23] K. Guo *et al.*, "Angel-eye: A complete design flow for mapping cnn onto embedded fpga," *IEEE TCAD*, vol. 37, no. 1, pp. 35–47, 2017.
- [24] X. Zhang *et al.*, "Dnnbuilder: An automated tool for building high-performance dnn hardware accelerators for fpgas," in *2018 IEEE/ACM ICCAD*. IEEE, 2018, pp. 1–8.
- [25] H. Ye *et al.*, "Hybriddnn: A framework for high-performance hybrid dnn accelerator design and implementation," in *2020 57th ACM/IEEE DAC*, 2020, pp. 1–6.
- [26] L. D. Bereholschi, C.-C. Lin, M. Yayla, and J.-J. Chen, "Hep-bnn: A framework for finding low-latency execution configurations of bnns on heterogeneous multiprocessor platforms," 2023.
- [27] C. Li *et al.*, "Pim-dl: Expanding the applicability of commodity dram-pims for deep learning via algorithm-system co-optimization," in *Proceedings of the 29th ACM International Conference on Architectural Support for Programming Languages and Operating Systems, Volume 2*, ser. ASPLOS '24. New York, NY, USA: Association for Computing Machinery, 2024, p. 879–896.
- [28] R. Kohavi *et al.*, "A study of cross-validation and bootstrap for accuracy estimation and model selection," in *IJCAI*, vol. 14, no. 2. Montreal, Canada, 1995, pp. 1137–1145.
- [29] E. Wang *et al.*, "Lutnet: Rethinking inference in fpga soft logic," in *2019 FCCM*. Los Alamitos, CA, USA: IEEE Computer Society, may 2019, pp. 26–34.
- [30] A. Ahmad and M. A. Pasha, "Optimizing hardware accelerated general matrix-matrix multiplication for cnns on fpgas," *IEEE TCS II: Express Briefs*, vol. 67, pp. 2692–2696, 2020.